Control and imaging of interfering wave packets in dissociating I_2 molecules

Christian Petersen, Emmanuel Péronne,* Jan Thøgersen, and Henrik Stapelfeldt†
Department of Chemistry, University of Århus, DK-8000 Århus C, Denmark

Mette Machholm‡
NORDITA, Blegdamsvej 17, DK-2100 Copenhagen Ø, Denmark
(Received 28 May 2004; published 16 September 2004)

Dissociation of iodine molecules by two phase-locked 110 femtosecond laser pulses creates a wave packet in the repulsive part of the *B* state. The time-dependent density functions for the internuclear position, $|\Psi(R,t)|^2$, and for the internuclear velocity, $|\Psi(v_R,t)|^2$, of the wave packet are measured by ionization with a delayed, intense 20 fs nonresonant laser pulse. The pronounced interference pattern, observed in both $|\Psi(R)|^2$ and $|\Psi(v_R)|^2$, is controlled by the time separation of the two pump pulses. The experimentally determined internuclear position and velocity distributions are in very good agreement with calculated results for $|\Psi(R)|^2$ and $|\Psi(v_R)|^2$ obtained by numerical wave packet propagation.

DOI: 10.1103/PhysRevA.70.033404 PACS number(s): 32.80.Qk, 33.80.Gj, 33.15.Bh, 34.50.Lf

I. INTRODUCTION

The formation and manipulation of wave packets in quantum systems are important both from a fundamental perspective as well as in the many emerging areas of quantum control at the atomic and molecular level [1–3,30]. The strong development in the ability to shape ultrashort laser pulses has essentially converted the field of wave packet dynamics from a discipline of passive observation of phenomena, i.e., spectroscopy, to a discipline of active manipulation. One particular type of wave packet control involves interference between wave packets, created by two or more ultrashort laser pulses.[1] It has proven a versatile and efficient approach for control and characterization in a variety of systems. These studies include interferometry of bound vibrational wave packets in small molecules [4–9], interferometry of electronic wave packets in Rydberg atoms [10–12,31], control of molecular chirality [13], and interference between freely expanding electrons [14] or internuclear wave packets [15,16].

In this paper we study numerically and experimentally the interference between two dissociative wave packets in molecular iodine. Two phase-locked 110 fs pump pulses create the wave packets by exciting the iodine molecules to the repulsive part of the *B* state. Experimentally, a delayed, intense 20 fs laser probe-pulse ionizes the dissociating molecules, and the internuclear density function, $|\Psi(R)|^2$, and the internuclear velocity density function, $|\Psi(v_R)|^2$, are determined from the kinetic energy distributions of the ionic fragments. We measure $|\Psi(R)|^2$ and $|\Psi(v_R)|^2$ as a function of time by varying the delay between the pump and the probe pulses.

The measured density functions $|\Psi(v_R)|^2$ and $|\Psi(R)|^2$ display strong oscillations due to interference of the two wave packets. The phase difference between the two pump pulses controls the interference pattern. In particular, the interference undergoes a π-phase shift as the delay between the excitation pulses is changed by half an optical period. The modulations are much more pronounced than in our first report on the subject [15], primarily because the pump pulses are now phase-locked. The structure of the measured $|\Psi(v_R)|^2$ and $|\Psi(R)|^2$ is in excellent agreement with the calculated distributions.

Our paper is organized in the following way. In Sec. II the basic idea of the experiment is described and the development of wave packet interference is illustrated by calculations. This section also contains a description of our numerical approach. The experimental setup is discussed in Sec. III. The experimental and numerical results are presented and compared in Sec. IV. The quantum nature of the wave packet interference is illustrated by calculated Wigner functions in Sec. V. Finally, Sec. VI contains concluding remarks.

II. DOUBLE PULSE DISSOCIATION OF A MOLECULE

A. Basic ideas: Development of interference

Figure 1(a) illustrates the basic idea of the experiment. Two identical pump laser pulses separated in time excite an iodine molecule from the electronic ground state to the continuum of the *B* state. Hereby, two dissociating wave packets are formed. Dispersion during the dissociation causes the wave packets to overlap and interfere. The relative amplitude and spacing of peaks in the interference pattern are determined by the time separation of the pump pulses.

The calculated internuclear density distributions $|\Psi(R)|^2$ in Fig. 1(c) illustrate the development of interference as a function of time, *t*, after the second pump pulse. Shortly after

*Present address: Laboratoire des Milieux Désordonnés et Hétérogénes, Université Pierre et Marie Curie, 75252 Paris Cedex 05, France.
†Electronic address: henriks@chem.au.dk
‡Also at Ørsted Laboratory, Niels Bohr Institute, University of Copenhagen, Denmark.

[1]Interfering internuclear wave packets can also be generated by predissociation of a diatomic molecule upon irradiation with a single femtosecond laser pulse—see Ref. [27].

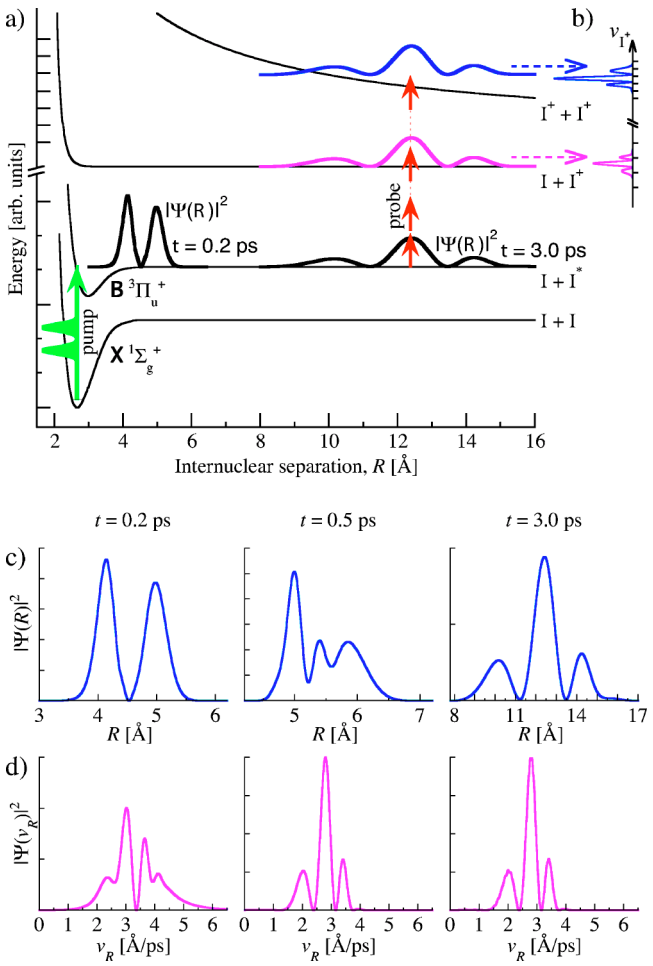

FIG. 1. Principle of the experiment and development of interference. (a) Energy diagram of I_2 showing both the potential curves involved in the wave packet formation and the potential curves used to measure $|\Psi(v_R)|^2$(I^+-I) and $|\Psi(R)|^2$(I^+-I^+) from the ion velocities as illustrated in (b). Above the *B*-potential curve and in (c), we show calculated $|\Psi(R)|^2$ for double pulse excitation, and in (d) the corresponding calculated $|\Psi(v_R)|^2$. The interference appears in $|\Psi(v_R)|^2$, as soon as the wave packet reaches the flat part of the *B*-potential curve (t=0.5 ps). Dispersion causes the initially separated parts of $|\Psi(R)|^2$ (t=0.2 ps) to overlap and interfere, and the final interference pattern is established at t=3.0 ps.

excitation, the two wave packets are separated on the potential curve. This is illustrated by the calculated $|\Psi(R)|^2$ at t =0.2 ps. The larger width of the peak centered around 5 Å shows that dispersion has already broadened the wave packet excited by the first pump pulse. At t=0.5 ps, the wave packets begin to overlap, and the interference pattern develops until a steady three-peaked structure is established (t=3.0 ps). At later times the relative magnitudes of the peaks remain unchanged, but each peak continues to spread out due to dispersion.

The double pulse excitation also produces interference in the internuclear velocity density distribution $|\Psi(v_R)|^2$, as illustrated by the calculated $|\Psi(v_R)|^2$ in Fig. 1(d). The wave packet created in the *B* state initially accelerates and subsequently slows down during passage of the short range potential well ($R<5$ Å). Therefore, shortly after excitation (t=0.2 ps) high internuclear velocities ($v_R>4$ Å/ps) are seen. As soon as both wave packets reach the flat part of the *B*-state potential ($t\geqslant 0.5$ ps) the high velocity components have disappeared, and the final interference structure for $|\Psi(v_R)|^2$ is established. At later times $|\Psi(v_R)|^2$ remains unchanged, since there is no force on the iodine fragments that can influence their relative velocity.

Comparison of $|\Psi(v_R)|^2$ and $|\Psi(R)|^2$ at t=0.5 ps shows that the interference develops first in $|\Psi(v_R)|^2$ and only later the steady structure of $|\Psi(R)|^2$ is reached. An interference pattern appears, if the wave packets overlap. The wave packets overlap completely in momentum space as soon as both wave packets reach the flat part of the *B*-state potential. On the other hand, the overlap in *R* space develops only gradually. For $t>3$ ps the overlap is essentially completed in *R* space.

To measure $|\Psi(R)|^2$ and $|\Psi(v_R)|^2$ at different times, the dissociating I_2 molecule is projected onto an $I+I^+$ or an $I^+ + I^+$ potential curve by multiphoton absorption from an intense ultrashort probe pulse delayed with respect to the pump pulses. For $R>10$ Å, the $I^+ + I^+$ potential curve is Coulombic and the $I+I^+$ potential curve is flat. The internuclear density function is obtained from the velocity distribution of the I^+ ions originating from the $I^+ + I^+$ channel [Fig. 1(b)] using Coulomb's law [17]. Likewise, the internuclear velocity density function $|\Psi(v_R)|^2$ is obtained from the velocity distribution of the I^+ ions originating from the $I+I^+$ channel. In particular, the velocity of the wave packet in the *B* state is the same as that in the $I+I^+$ channel, since both potentials are essentially flat for $R>10$ Å.

For internuclear distances below 8–10 Å the $I^+ + I^+$ potential curves start to deviate from a Coulombic shape and the $I+I^+$ potential curves deviate from the flat form. This introduces an error in the experimental determination of $|\Psi(v_R)|^2$ and $|\Psi(R)|^2$—the error becoming gradually larger as *R* is lowered. As a result, we only present experimental data for $R>10$ Å, corresponding to $t\geqslant 3$ ps.

B. Numerical approach

We have performed numerical simulations of the wave packet dynamics of the system. The theoretical model includes two molecular states: the ground $X\ ^1\Sigma_g^+$ state and the excited $B\ ^3\Pi_u^+$ state of I_2.[2] The pump laser induces a coupling of the *X* state and the *B* state. In the dipole approximation the coupling is $V_{\text{pump}}(R)=\boldsymbol{\mu}(R)\cdot\mathbf{E}_{\text{pump}}(t)$. The excitation is very localized in *R*, and the transition dipole moment $\boldsymbol{\mu}$ may be assumed constant. The Rabi coupling $\Omega_R=\mu E_0/\hbar$ is adjusted so that only a few percent of the ground state population is transferred to the excited state.

The pump pulses are identical and separated by the delay τ_{pump} so the total pump field, $E_{\text{pump}}(t)$, can be expressed as

$$E_{\text{pump}}(t) = E(t+\tau_{\text{pump}}) + E(t), \tag{1}$$

where $E(t+\tau_{\text{pump}})$ denotes the field of the first pump pulse. To model the experimental pump pulses, $E(t)$ is expressed by a chirped Gaussian pulse [18],

[2]We use the analytical potentials for the *X* and *B* states given by Che *et al.* [29].

$$E(t) = \frac{E_0}{\gamma^{1/4}} e^{-t^2/\beta\gamma} \cos(\omega t - \delta t^2 - \varepsilon), \tag{2}$$

where

$$\beta = \frac{T_{\text{pump}}^2}{2\ln 2}, \quad \gamma = 1 + \frac{4\phi''^2}{\beta^2}, \quad \delta = \frac{2\phi''}{\beta^2\gamma}, \quad \varepsilon = \frac{1}{2}\arctan\frac{2\phi''}{\beta}. \tag{3}$$

The corresponding unchirped pulse has a peak amplitude E_0, and a FWHM of the intensity profile T_{pump}. ω is the central angular frequency and ϕ'' is the linear chirp of the pulse. In the experiment the pump pulse length, $T_{\text{pump}}\gamma^{1/2}$, is typically 110 fs. The spectral width of the pump pulses corresponds to a Fourier transform limited pulse with a duration in the range 65 to 90 fs.

The time-dependent one-dimensional Schrödinger equation for the coupled X and B states is solved on a grid using wave packet calculations with a splitting of the short-time propagator [19,20] and a fast Fourier transformation between coordinate $\Psi(R)$ and momentum $\Psi(k)$ representations. The internuclear density function $|\Psi(R,t)|^2$ for the wave packet in the B state is obtained after propagation to the desired pump-probe delay t. The internuclear velocity density function $|\Psi(v_R,t)|^2$ is calculated from $\Psi(k)$ in the B state.

The discrete representations of the stationary vibrational eigenstate wave functions, either the $X(v=0)$ or the $X(v=1)$ states, are used as initial conditions for the propagations. For comparison with the experiments we calculate the incoherent sums

$$\sum_{v=0,1} \alpha_v |\Psi_v(R,t)|^2 \quad \text{and} \quad \sum_{v=0,1} \alpha_v |\Psi_v(v_R,t)|^2. \tag{4}$$

The weight factors α_v in the incoherent sums are determined by the initial vibrational state populations of the molecules in the experiment. The calculated density distributions for the wave packets in the B state are compared to the measured distributions in Sec. IV (see Figs. 3 and 4).

III. EXPERIMENTAL SETUP

Most of the experimental setup has been described previously [15] and only the important features are discussed here. A pulsed molecular beam is formed by expanding 1 mbar iodine in 3 bar helium and crossed at 90° by two focused laser beams.

The laser beam containing the pump pulses for the photoexcitation of I_2 is produced by sum frequency mixing the signal output from a fs optical parametric amplifier (TOPAS) with part of the output from an amplified fs Ti-sapphire laser ($\lambda = 800$ nm). The parametric amplifier is operated around $\lambda = 1300$ nm giving the pump pulses a wavelength of ~495 nm.

Each of the frequency mixed pulses is split into two pulses by passing them through a phase-locked Michelson interferometer [21]. The pump pulse separation, τ_{pump}, can be adjusted in steps of 0.315 fs. The final pump pulses are ~110 fs long. Each pulse contains ~2.5 μJ of energy, and the pump beam is focused to a spot size $\omega_0 \sim 31$ μm, so the peak intensity of each pump pulse is $\sim 1.5 \times 10^{12}$ W/cm^2.

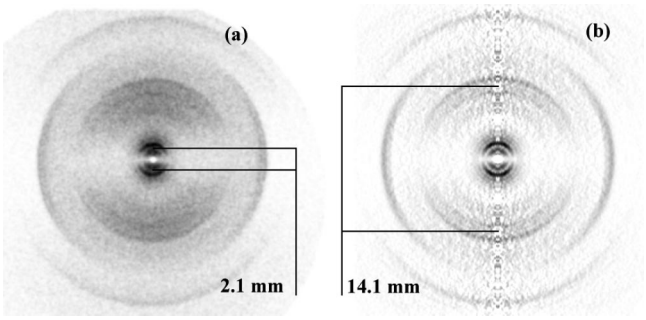

FIG. 2. (a) The raw I^+ image recorded for a pump wavelength of 494.5 nm, $\tau_{\text{pump}} = 294.55$ fs and $t = 10.4$ ps. It is the sum of 20 000 individual images (20 000 laser shots) and contains a total of 380 000 ion hits. (b) The Abel inverted image corresponding to the raw image in (a).

The phase locking is done by passing a HeNe laser ($\lambda = 632.8$ nm) through the interferometer collinear with the pump laser beam. One of the end mirrors of the Michelson interferometer is mounted on a piezocrystal. We use the error signal from the HeNe interference to control the piezocrystal. This mechanism allows for a stabilization of the interferometer on the order of $\sim\pi/8$ and is the main improvement of the experimental setup compared to Ref. [15].

The probe pulses, making up the second laser beam, are created by sending the rest of the amplified Ti-sapphire laser output through a home-built hollow core wave guide compressor. The probe pulse is delayed by t with respect to the second pump pulse. The pulses are compressed such that their duration, T_{probe}, is ~25 fs inside the vacuum chamber where their pulse energy is adjusted to ~54 μJ. With a focal spotsize $\omega_0 \sim 27$ μm the peak intensity reaches $\sim 1.9 \times 10^{14}$ W/cm^2.

The ions, produced in the laser-molecule interaction, are detected by two-dimensional (2D) ion imaging. Fast gating of the ion detector (Microchannel plates) ensures that the 2D ion images only contain ions with a mass-to-charge ratio equal to that of I^+. Typically, 15–25 ions are detected in each individual image and a total "raw" image is the sum of 15–20 000 individual images. An example of a raw image, recorded for $\tau_{\text{pump}} = 294.55$ fs and $t = 10.4$ ps, is shown in Fig. 2(a). Since the polarizations of both the pump and the probe laser beams are collinear and parallel to the plane of the detector any raw image recorded in the experiment can be Abel inverted.[3] Hereby, the kinetic energy distribution (and the angular distribution) of the I^+ ions, can be determined [22]. Figure 2(b) is the Abel inverted image of the raw image in Fig. 2(a). On the vertical center line of the Abel inverted image the noise originating from the Abel inversion can be seen. This center line is disregarded when the kinetic energy distributions are determined from the image.

[3]We use the Basex procedure for the Abel inversion—see Ref. [28].

IV. RESULTS AND DISCUSSION

A. Extraction of the measured $|\Psi(v_R)|^2$ and $|\Psi(R)|^2$

The images in Fig. 2 exhibit two pairs of half rings, one with a diameter of ~2.1 mm and one with a diameter of ~14.1 mm. The innermost pair of half rings are produced when the intense probe pulse projects the dissociating wave packet onto an I^+-I potential curve, i.e., single ionization of the dissociating molecule. The outermost pair of half rings result from the wave packet being projected onto an I^+-I^+ potential curve, i.e., double ionization of the dissociating molecule. The substructure in each pair of half rings is only observed when two pump pulses are used. It is the signature of interference between the two wave packets created by the two pump pulses as shown previously [15].

To extract $|\Psi(v_R)|^2$ and $|\Psi(R)|^2$ from the experimental data the following procedure is applied. From the radial distribution of each Abel inverted image recorded with the pump and probe pulses we subtract the radial distribution of an Abel inverted image recorded with only the probe pulse. The latter radial distribution is scaled by an experimentally determined factor (<1) to compensate for the fact that the pump pulses dissociate a non-negligible fraction of the molecules. The part of the resulting radial distribution corresponding to the I^+-I channel is directly converted into a distribution of internuclear velocities to obtain $|\Psi(v_R)|^2$.

Similarly, the part of the radial distribution corresponding to the I^+-I^+ channel is converted into a distribution of kinetic energies, $P(E_{\mathrm{kin}})$ including the appropriate probability transformation of the radial distribution. Energy conservation gives

$$P(E_{\mathrm{kin}}) = \int P(E_{\mathrm{dis}})P(E_{\mathrm{Coul}} = E_{\mathrm{kin}} - E_{\mathrm{dis}})dE_{\mathrm{dis}}, \qquad (5)$$

where $P(E_{\mathrm{dis}})$ and $P(E_{\mathrm{Coul}})$ are the probability distributions of the dissociation and the Coulomb energies, respectively. Since $P(E_{\mathrm{dis}})$ is obtained from $|\Psi(v_R)|^2$ we can extract $P(E_{\mathrm{Coul}})$ by deconvolution of $P(E_{\mathrm{kin}})$ from $P(E_{\mathrm{dis}})$. Hereafter, the distribution of internuclear distances, $|\Psi(R)|^2$, is determined using Coulomb's law and, again, transformation of the probability distributions [17].

B. Phase control of the interference pattern

Figure 3 displays the R distribution of the interfering wave packets obtained at three different probe times. The corresponding v_R distribution is approximately the same at three different times [Fig. 3(d), (D)]. The central wavelength of the pump pulses is 494.5 nm and on each subfigure the results obtained for $\tau_{\mathrm{pump}}=305.0$ fs and 306.0 fs are shown. The experimentally recorded R distributions exhibit three major interference peaks for $\tau_{\mathrm{pump}}=305.0$ fs and two major peaks for $\tau_{\mathrm{pump}}=306.0$ fs [Figs. 3(a) and 3(d)] in good agreement with the calculated results [Figs. 3(a)–3(c)]. The relative magnitudes of the experimental interference peaks are essentially the same at the three different delays, but each peak broadens due to dispersion. For instance, the FWHM of the largest peak on the full curve increases from ~2.0 Å at $t=5.9$ ps [Fig. 3(a)] to ~3.4 Å at $t=9.9$ ps [Fig. 3(c)]. The broadening of the interference peaks also agrees well with the calculations.

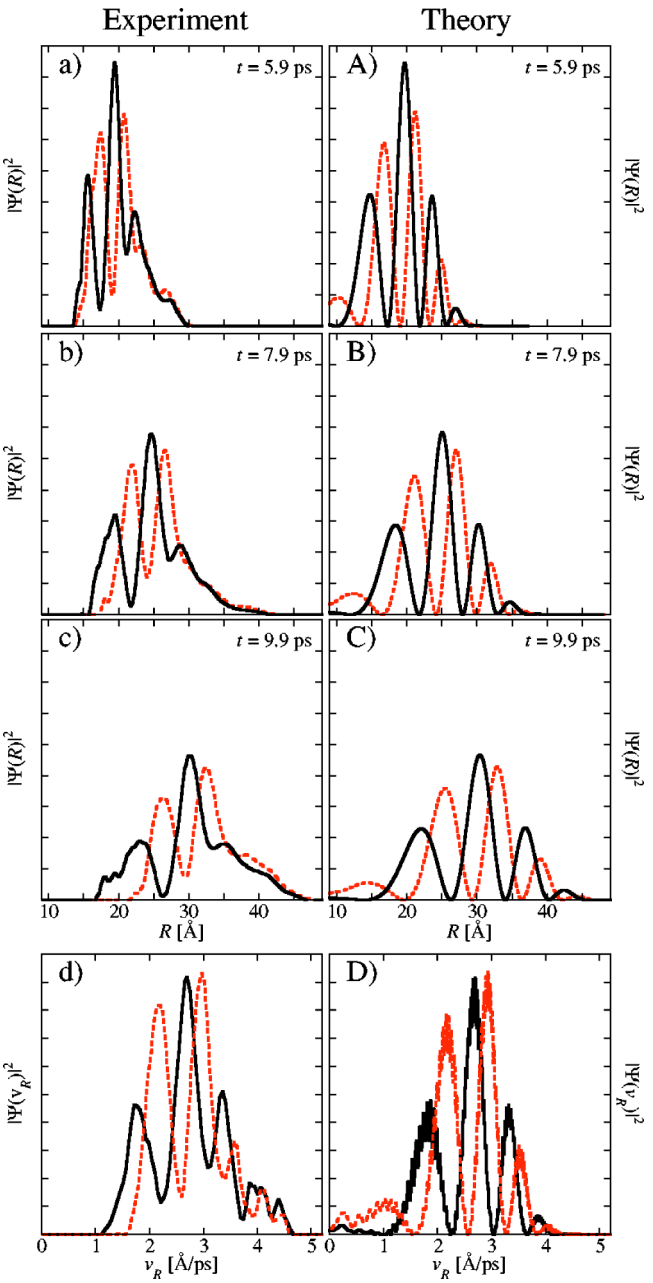

FIG. 3. $|\Psi(R)|^2$ and $|\Psi(v_R)|^2$ measured (left column) and calculated (right column) at three different probe times and for two different pump-pump delays. On each figure the probe time, t, is given, and the full curve corresponds to $\tau_{\mathrm{pump}}=305.0$ fs and the dashed curve to $\tau_{\mathrm{pump}}=306.0$ fs. The velocity distribution is the same for all three delays and shown in (d) and (D). The calculated distributions (A)–(D) contain contribution only from molecules initially in the vibrational ground state, $v=0$. The fast jitter in the calculated $|\Psi(v_R)|^2$ is due to a small coherent population of the bound vibrational states of the B state.

Comparing the R distributions obtained with $\tau_{\mathrm{pump}}=305.0$ fs and 306.0 fs we see that the interference structure undergoes a phase shift slightly larger than π. The reason is that the Michelson interferometer is locked to either the "bot-

tom" ($\tau_{\text{pump}}=305.0$ fs) or the "top" ($\tau_{\text{pump}}=306.0$ fs) of the interference fringes from a HeNe laser. The time difference between "top" and "bottom" is half an optical period at 632.8 nm, ~1.0 fs, which is ~1.28 times half an optical period at 494.5 nm, i.e., a phase shift of 1.28π.

The complete modulation of the calculated $|\Psi(R)|^2$ is not perfectly reproduced by the experimental observations. However, the experimental modulation of $|\Psi(R)|^2$ is much stronger than the modulation in our first report on interference between dissociating wave packets [15]. In fact, $|\Psi(R)|^2$ almost reaches zero between the two largest interference peaks on the full curves [Figs. 3(a)–3(c)]. The improvement is primarily caused by the phase locking of the two pump pulses in the present work. The lack of phase locking in our previous work [15] caused phase fluctuation and phase drift, during the recording of an ion image, that were sufficiently large to blur the interference structure although still small enough for the appearance of clear interference structures.

Pronounced interference structures are also observed in the internuclear velocity distributions [Fig. 3(d)]. For $\tau_{\text{pump}}=305.0$ fs four individual peaks are resolved. Their positions at 1.77, 2.69, 3.36, 3.97 Å/ps agree well with the positions of the peaks in the calculation, 1.83, 2.70, 3.33, 3.88 Å/ps [Fig. 3(d)]. Similarly, for $\tau_{\text{pump}}=306.0$ fs the positions of the experimentally observed interference peaks, 2.18, 2.97, 3.58, 4.14 Å/ps, are in good agreement with the calculated positions (2.18, 2.93, 3.56, 4.08 Å/ps). At both pump-pump delays the relative magnitudes of the interference peaks predicted by the calculations are very well reproduced by the experimentally measured v_R distributions.

C. Spectrum of the pump pulses

The peaks in $|\Psi(R)|^2$ and in $|\Psi(v_R)|^2$ are correlated in the sense that each interference peak in $|\Psi(R)|^2$ moves with a velocity given by the corresponding peak in $|\Psi(v_R)|^2$. To illustrate the correlation we determined the average velocity of the peaks in the experimental R distributions by plotting their central positions as a function of the three probe times in Fig. 3. For each peak the three points fall on a straight line as expected for the linear motion of the dissociating molecule. With $\tau_{\text{pump}}=305.0$ fs we find 1.83, 2.70, and 3.25 Å/ps in good agreement with the peak positions in $|\Psi(v_R)|^2$ noted above. Similarly, for $\tau_{\text{pump}}=306.0$ fs we find 2.23 and 2.93 Å/ps, which agree well with the central positions of the two peaks with the smallest velocities in the v_R distribution.

To understand the interference pattern in $|\Psi(v_R)|^2$ we note that once the wave packets have reached the flat part of the B-state potential the distribution of the dissociation energies, $P(E_{\text{dis}})$, is determined by the spectrum of the pump-pulses $S(\omega)$ and the Franck-Condon factor $F_{\text{FC}}(\omega)$:

$$P(E_{\text{dis}}) \propto S(\omega)F_{\text{FC}}(\omega). \tag{6}$$

The spectrum of the two identical pump-pulses, separated by τ_{pump} is

$$S(\omega) = (1+\cos(\omega\tau_{\text{pump}}))S_{\text{pump}}(\omega), \tag{7}$$

where $S_{\text{pump}}(\omega)$ is the spectrum of a single pump pulse. Thus, the spectral modulation of $1/\tau_{\text{pump}}$ [Eq. (7)] is directly transferred to $P(E_{\text{dis}})$ and therefore also to $|\Psi(v_R)|^2$. The Franck-Condon factor, accounting for the energy dependence of the overlap between the initial vibrational level and the final continuum state, does not produce interference but rather a small modification of the envelope of $P(E_{\text{dis}})$ compared to the envelope of $S(\omega)$.

The interference structure in $|\Psi(R)|^2$ can now be thought of as being created by the structured internuclear velocity distribution, i.e., each interference peak in $|\Psi(R)|^2$ moves with a velocity given by the corresponding interference peak in $|\Psi(v_R)|^2$. We note that the final distribution of dissociation energies and therefore $|\Psi(v_R)|^2$ is only determined by the spectrum of the pulses [23]. On the other hand, $|\Psi(R)|^2$ also depends strongly on the pulse duration and the chirp of the pump pulses. For instance, the dissociating wave packets may be focused (minimizing the width) at a chosen R, if the pump pulses are properly positively chirped [24].

D. Comparison of calculated and measured distributions

Another example of our ability to image the dissociative wave packet is displayed in Fig. 4. Here, we show measurements and calculations of $|\Psi(R)|^2$ at seven different probe times for a fixed pump-pump delay. In this time interval the wave packet evolves from a mean internuclear distance of 13.9 Å at $t=3.4$ ps to 30.0 Å at 9.4 ps. The figure also shows $|\Psi(v_R)|^2$ which is approximately the same for all the probe times ($3.4\ \text{ps} \leqslant t \leqslant 9.4$ ps) considered.

Overall, the agreement between the experimental and the calculated results is gratifying. In particular, the position and the relative magnitude of the two major interference peaks in the experimental R distributions overlap precisely with the calculated $|\Psi(R)|^2$'s at all times.[4] The broadening of the wave packet due to dispersion is also clearly illustrated in the experimental data. For instance, the FWHM increases from 1.3 Å at $t=3.4$ ps to 5.0 Å at $t=9.4$ ps in good agreement with the calculations.

The calculated distributions have an initial vibrational state distribution of 90% in $v=0$ and 10% in $v=1$ of the X state. The two main peaks at the smaller values of R originate from molecules initially in $v=0$. The third peak has contributions from both $v=0$ and $v=1$, whereas the two peaks located at the largest values of R mainly contain contributions from $v>0$. Experimentally, the interference structure is very well resolved for the $v=0$ contribution. The peaks at the largest R values, visible for each probe delay in the calculated $|\Psi(R)|^2$'s, are only partly observed experimen-

[4] At $t=3.4$ ps the experimental relative magnitude of the two major interference peaks deviate slightly from the calculated and also from the relative magnitude at other times. This is most likely caused by imperfect phase locking of the two pump pulses during the recording at 3.4 ps.

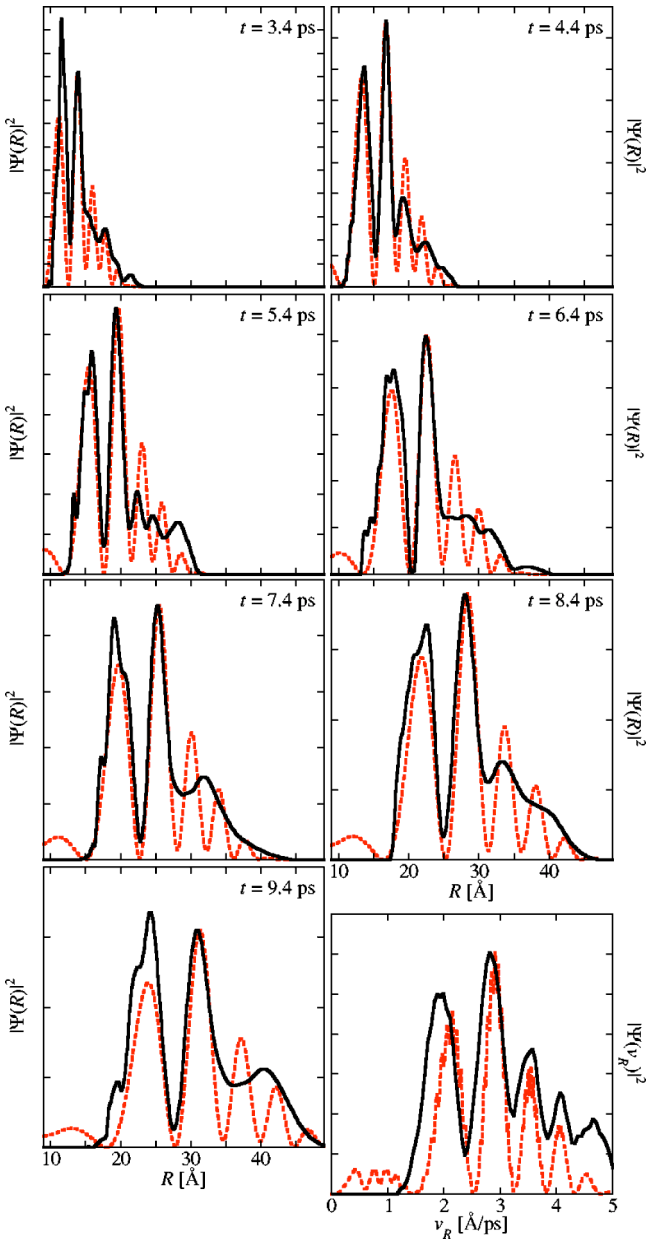

FIG. 4. $|\Psi(R)|^2$ and $|\Psi(v_R)|^2$ measured (full curves) and calculated (dashed curves) at seven different probe times. The wavelength of the pump pulses is 494.5 nm and $\tau_{\text{pump}}=294.55$ fs. The velocity distribution is approximately the same for all probe delays and the average is shown in the lower right-hand figure.

tally. This lack of resolution could originate from imperfections in our ion imaging technique.[5]

Comparing the calculated and the measured $|\Psi(v_R)|^2$, it is seen that all four significant interference peaks are resolved experimentally but there is a small offset between the experimental and the calculated peak positions. The precise peak positions are very sensitive to the precise phase of the two pump pulses. Any small deviation in the value of τ_{pump} used in the calculation from the real τ_{pump} in the experiment will cause a shift of the peak positions.

[5]The finite duration of the probe pulse induces an R-blur of $\sim T_{\text{probe}} v_R$ as the wave packet is projected onto a Coulomb curve. Although the peaks at large R originate from the fastest part of the wave packet, v_R is still less than 5 Å/ps meaning that the upper limit on the R-blur in the probe step is 5×0.025 Å ≈ 0.13 Å. Therefore, the origin of the limitations in the imaging technique is more likely found in the velocity focusing and detection of the ions.

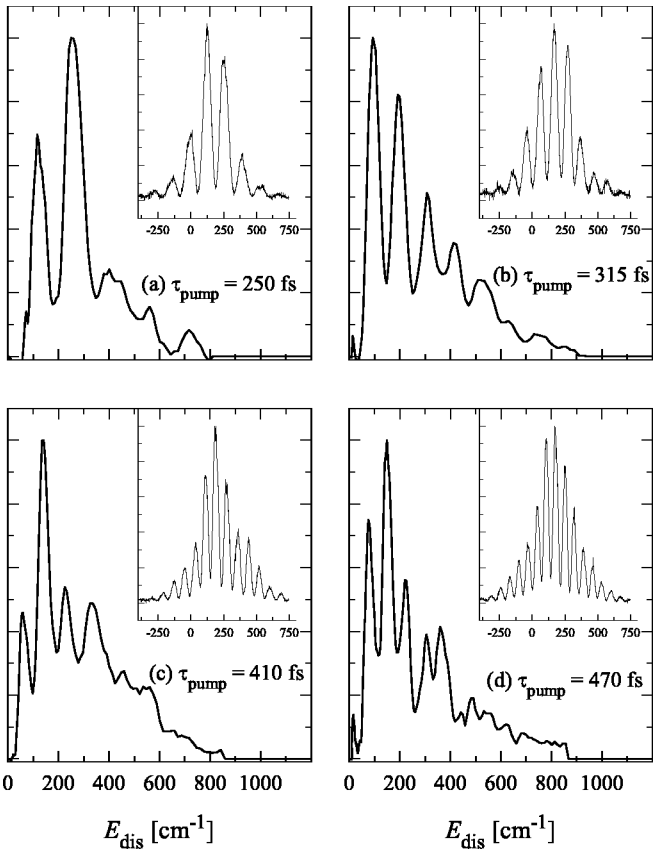

FIG. 5. The distribution of dissociation energies, $P(E_{\text{dis}})$, recorded at four different pump-pump delays. For each τ_{pump} the corresponding spectrum of the two pump pulses is shown as an inset.

Both the spectral width and the duration of the pump pulses have been taken into account for the pump pulses used in the calculations. With the present parameters the main effect of the chirp of the pump pulses is additional width of the peaks in $|\Psi(R)|^2$ compared to a calculation with 65 fs Fourier transform limited Gaussian pulses.

E. Dependence on pump-pump delay

The data presented so far were obtained for a pump-pump delay around 300 fs. To illustrate the dependence of the wave packet interference upon the pump-pump delay we recorded $|\Psi(v_R)|^2$ and $|\Psi(R)|^2$ for different values of τ_{pump}. The results are displayed in Figs. 5 and 6. We plot the distribution of dissociation energies, $P(E_{\text{dis}})$ rather than $|\Psi(v_R)|^2$ to provide a direct comparison with the corresponding optical spectra (Fig. 5). As τ_{pump} is increased from 250 to 470 fs the modulation period in the optical spectrum is observed to decrease from 133 cm^{-1} to 71 cm^{-1} in excellent agreement with the $1/\tau_{\text{pump}}$ modulation expected from Eq. (7).

Qualitatively, the dependence of the modulation period upon τ_{pump} is clearly reproduced in $P(E_{\text{dis}})$ as seen in Fig. 5.

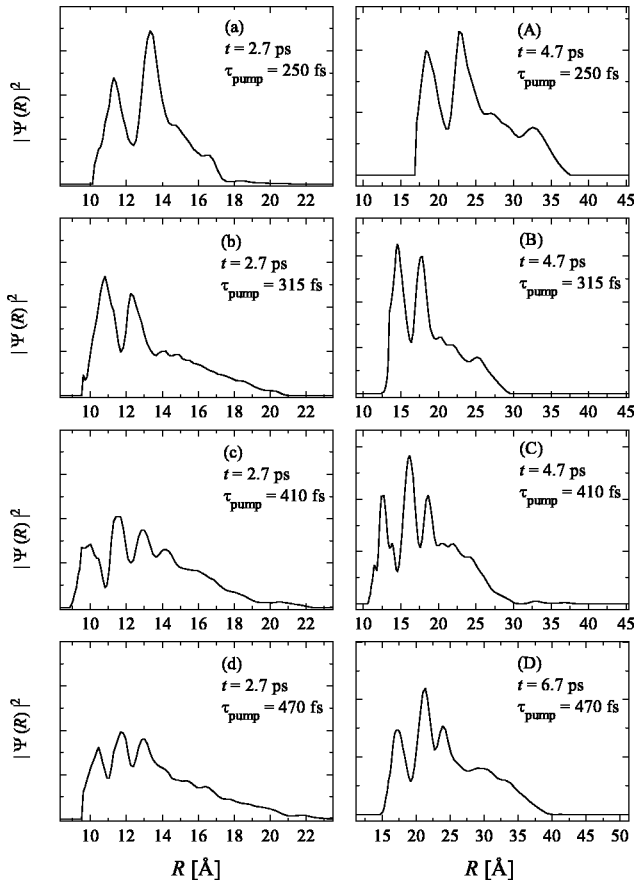

FIG. 6. $|\Psi(R)|^2$ measured for four different pump delays. The distributions are shown for two probe delays in each case to confirm the interference structure. The spacing between the interference peaks becomes smaller at larger pump delays.

To provide a quantitative comparison we measure the spacing between the major interference peaks, located at the lowest dissociation energies ($E_{\mathrm{dis}}<300$ cm^{-1}) because this part of $P(E_{\mathrm{dis}})$ is produced by dissociation of molecules in the $v=0$ level. The high kinetic part has contributions both from molecules in the $v=0$ level, dissociated by the high energy part of the spectrum, and from molecules in excited vibrational states (mainly $v=1$ and 2) dissociated by the low energy part of the spectrum. In general, when the vibrational spacing ($\sim$210 cm^{-1}) differs from an integer multiplum of the spectral modulation these contributions will blur $P(E_{\mathrm{dis}})$ at large dissociation energies. The results for the modulation period of the four different $P(E_{\mathrm{dis}})$, summarized in Table I, agree very well with the modulation observed in the corresponding optical spectra.

Figure 6 shows $|\Psi(R)|^2$ at two different probe times for the four different τ_{pump}. Similar to the observations in $P(E_{\mathrm{dis}})$ we detect a decrease in the modulation period as τ_{pump} increases. For instance, at $t=2.7$ ps the fringe spacing is $\sim$2.0 Å for $\tau_{\mathrm{pump}}=250$ fs and only $\sim$1.2 Å for $\tau_{\mathrm{pump}}=470$ fs. In each of the R-distributions measured we only resolve clear interference peaks at the smallest internuclear distances because this part has a contribution only from $v=0$. For the same reason as given in the discussion of Fig. 5 the large R part of the R distributions is blurred due to contributions from wave packets excited from different vibrational states.

TABLE I. The modulation frequency of the four dissociation energy distributions and optical spectra shown in Fig. 5.

τ_{pump}	250 fs	315 fs	410 fs	470 fs
E_{dis} modulation (cm^{-1})	134	101	86	73
Spectral modulation (cm^{-1})	133	110	81	71

The spacing between the peaks in Fig. 6(d) corresponds to an internuclear resolution of 1.2 Å in the internuclear region $\sim$10–14 Å. In the present experiments we did not perform experiments with a larger pump-pump delay than 470 fs. We note, however, that finer modulation of both $|\Psi(v_R)|^2$ and $|\Psi(R)|^2$ resulting from even larger values of τ_{pump} provides a way of calibrating the resolution of the wave packet imaging.

V. WIGNER FUNCTIONS OF INTERFERING WAVE PACKETS

In this section we represent calculated Wigner functions for the interfering wave packets to illustrate the quantum nature of the system. The Wigner function for two conjugate variables x and p,

$$W(x,p)=\frac{1}{\pi\hbar}\int \psi^*(x-x')\psi(x+x')e^{2ipx'/\hbar}\,dx', \qquad (8)$$

is a real function, but contains all information about the quantum state of the system. $W(x,p)$ is a quasiprobability function and features areas of negative probability $W(x,p)<0$, which are signatures of a coherent interfering quantum system.

Figure 7 shows Wigner functions $W(R,v_R)$ corresponding to the two dissociative wave packets in I_2. Here, W is given as a function of v_R instead of momentum for easier comparison with the v_R distributions discussed in this papers. Figure 7(a) represents the same state as Fig. 1 at $t=3$ ps. The full contours (red areas) correspond to positive values of $W(R,v_R)$. The coherent quantum nature of the system is evident, since areas with negative values of $W(R,v_R)$ are present (shown as dashed contours/blue areas). For comparison, the Wigner function for an incoherent sum of two dissociating wave packet are shown in Fig. 7(b). In the latter case $W(R,v_R)>0$ for all values of R and v_R. We include Fig. 7(b) to illustrate that each wave packet corresponds to an elongated peak along a line $R\propto v_R$. The two elongated peaks are nearly parallel. In the coherent case [Fig. 7(a)] these peaks are also present, but in between these peaks areas of positive and negative $W(R,v_R)$ appear due to interference.

Detection of the quantum state of a system might be realized through the implementation of a quantum tomography scheme. Quantum state tomography has been demonstrated for wave packets in bound states. In a harmonic potential the time evolution of $W(R,v_R)$ is a simple rotation of the phase-space distribution. In this case quantum tomography requires a series of measured marginal distributions, e.g., R distributions, for a full period of the motion in the bound state [25].

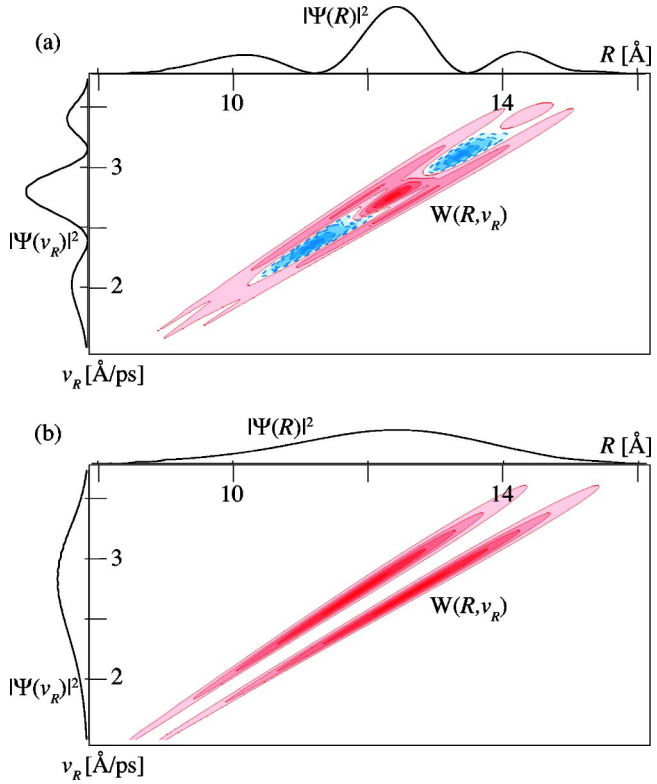

FIG. 7. Wigner function $W(R,v_R)$ for the dissociative wave packets created by double pulse excitation. Full contours (red), $W(R,v_R)>0$. Dashed contours (blue), $W(R,v_R)<0$. (a) Coherent double pulse excitation corresponding the calculated wave packet in Fig. 1 at $t=3$ ps. The areas with $W(R,v_R)<0$ is a signature of the interference. (b) Incoherent double pulse excitation. Only the two density islands corresponding to the individual wave packets are present.

For the freely propagating wave packet, time evolution dictates a shearing of the phase-space distribution. Even if we in principle were able to measure the R distributions at all probe delays this would only correspond to information on the phase-space distribution for a quarter rotation. This means that alternative methods of quantum tomography have to be implemented. The scheme of maximum entropy has been successfully used for quantum state tomography of molecules dissociated by only one laser pulse [26]. However, the inherent complex structure of the presently measured distributions provides a more demanding challenge. The distributions presented in Fig. 4 change very little for the various probe delays, and it is therefore likely that the information contained in our data is insufficient to allow for a reliable reconstruction of the quantum state. More realistic, it would be necessary to record the R distribution at the time where the width of the wave packet is minimized at the early times where the final interference structure is established (see Fig. 1). Unfortunately, our experimental technique is not suited for precise determination of $|\Psi(R)|^2$ at these small internuclear distances.

An alternative is to use positively chirped pump pulses. Hereby, the wave packets could be focused at sufficiently large internuclear distances that the Coulomb explosion technique enables determination of $|\Psi(R)|^2$ around the focus point. This would correspond to measurement of R distributions for an increased range of rotations of the phase-space distribution.

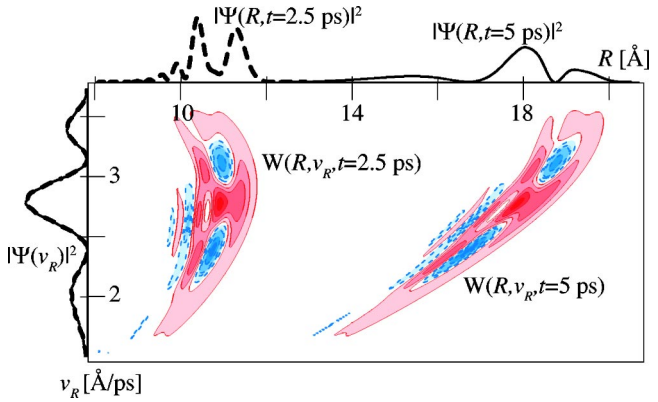

FIG. 8. Wigner function $W(R,v_R)$ for double pulse excitation with positively chirped pulses. The Wigner function corresponds to that in Fig. 7 except for the additional positive chirp of the pulses. The chirp stretches the pulses by a factor of 10, corresponding to a linear chirp $\phi''=2.9\times10^4$ fs^2 [Eq. (3)]. Full contours (red), $W(R,v_R)>0$. Dashed contours (blue), $W(R,v_R)<0$.

To illustrate our idea we calculated the Wigner functions when two positively chirped pump pulses create the dissociative wave packet (see Fig. 8). The chirp of the pump-pulses causes the wave packets to focus around 10 Å. The figure shows how the Wigner function is rotated by approximately 45° from $t=2.5$ ps to $t=5.0$ ps. The corresponding R-distributions, displayed in the upper panel of Fig. 8, exhibit very different interference patterns. We believe this increased information makes it possible to reconstruct the Wigner function from R distributions measured for a range of times around the focus time.

VI. CONCLUSION

The interference between two dissociating wave packets in molecular iodine was studied numerically and experimentally. In particular, $|\Psi(R)|^2$ and $|\Psi(v_R)|^2$, measured by Coulomb exploding the dissociating molecule with an intense 20-fs-long probe pulse, agreed very well with the calculated distributions. Experimentally, we illustrated the influence of the delay between the two pump pulses on the wave packet interference pattern. This provides a method for calibrating the internuclear position and velocity resolution of the experimental technique. The potential for determining the Wigner function, i.e., the full quantum information of the dissociative motion, was discussed.

ACKNOWLEDGMENTS

The authors thank all of the excellent technical staff members at the Chemistry and Physics Departments. This work was supported by the Carlsberg Foundation and the Danish Natural Science Research Council (SNF). The authors thank Hanna Reisler for providing us a program to perform Abel inversion.

[1] A. Stolow, Philos. Trans. R. Soc. London, Ser. A **356**, 345 (1998).
[2] T. Seideman, in *Computational Molecular Spectroscopy*, edited by P. Jensen and P. R. Bunker (Wiley, New York, 2000).
[3] L. E. E. Araujo and I. A. Walmsley, J. Opt. B: Quantum Semiclassical Opt. **5**, R27 (2003).
[4] N. F. Scherer, R. J. Carlson, A. Matro, M. Du, A. J. Ruggiero, V. Romero-Rochin, J. A. Cina, G. R. Fleming, and S. A. Rice, J. Chem. Phys. **95**, 1487 (1991).
[5] V. Blanchet, M. A. Bouchene, and B. Girard, J. Chem. Phys. **108**, 4862 (1998).
[6] M. A. Bouchene, C. Nicole, and B. Girard, J. Phys. B **32**, 5167 (1999).
[7] J. A. Cina, J. Chem. Phys. **113**, 9488 (2000).
[8] I. D. Pinkas, G. Knopp, and Y. Prior, J. Chem. Phys. **115**, 236 (2001).
[9] K. Ohmori, Y. Sato, E. E. Nikitin, and S. A. Rice, Phys. Rev. Lett. **91**, 243003 (2003).
[10] M. W. Noel and J. C. R. Stroud, Phys. Rev. Lett. **75**, 1252 (1995); **77**, 1913 (1996).
[11] L. D. Noordam, D. I. Duncan, and T. F. Gallagher, Phys. Rev. A **45**, 4734 (1992).
[12] T. C. Weinacht, J. Ahn, and P. H. Bucksbaum, Phys. Rev. Lett. **80**, 5508 (1998).
[13] J. A. Cina and R. A. Harris, Science **267**, 832 (1995).
[14] M. Wollenhaupt *et al.*, Phys. Rev. Lett. **89**, 173001 (2002).
[15] E. Skovsen, M. Machholm, T. Ejdrup, J. Thøgersen, and H. Stapelfeldt, Phys. Rev. Lett. **89**, 133004 (2002).
[16] B. M. Garraway and S. Stenholm, Phys. Rev. A **46**, 1413 (1992).
[17] H. Stapelfeldt, E. Constant, H. Sakai, and P. B. Corkum, Phys. Rev. A **58**, 426 (1998).
[18] S. D. Silvestri, P. Laporta, and O. Svelto, IEEE J. Quantum Electron. **QE-20**, 533 (1984).
[19] M. J. Feit, J. A. Fleck, and A. Steiger, J. Comput. Phys. **47**, 412 (1982).
[20] R. W. Heather, Comput. Phys. Commun. **63**, 446 (1991).
[21] C. Petersen, Master's thesis, Department of Chemistry, University of Aarhus, 2004.
[22] M. D. Poulsen, E. Skovsen, and H. Stapelfeldt, J. Chem. Phys. **117**, 2097 (2002).
[23] R. R. Jones, D. W. Schumacher, T. F. Gallagher, and P. H. Bucksbaum, J. Phys. B **28**, L405 (1995).
[24] B. Kohler, V. V. Yakovlev, J. Che, J. L. Krause, M. Messina, K. R. Wilson, N. Schwentner, R. M. Whitnell, and Y. Yan, Phys. Rev. Lett. **74**, 3360 (1995).
[25] T. J. Dunn, I. A. Walmsley, and S. Mukamel, Phys. Rev. Lett. **74**, 884 (1995).
[26] E. Skovsen, H. Stapelfeldt, S. Juhl, and K. Mølmer, Phys. Rev. Lett. **91**, 090406 (2003).
[27] J. Degert, C. Meier, B. Chatel, and B. Girard, Phys. Rev. A **67**, 041402 (2003).
[28] V. Dribinski, A. Ossadtchi, V. Mandelshtam, and H. Reisler, Rev. Sci. Instrum. **73**, 2634 (2002).
[29] J. Che, J. L. Krause, M. Mesina, K. R. Wilson, and Y. Yan, J. Phys. Chem. **99**, 14949 (1995).
[30] J. R. R. Verlet and H. H. Fielding, Int. Rev. Phys. Chem. **20**, 283 (2001).
[31] R. S. Minns, R. Patel, J. R. R. Verlet, and H. H. Fielding, Phys. Rev. Lett. **91**, 243601 (2003).